sustainability

MDPI

Article

Effects of Different Nitrogen Sources on the Formation of Biogenic Jarosite

Haitao Huang [1,2], Weitong Hu [1], Xiang Zi [1], Xiaomeng Wang [1], Jianru Liang [1] and Lixiang Zhou [1,*]

[1] Department of Environmental Engineering, College of Resources and Environmental Sciences, Nanjing Agricultural University, Nanjing 210095, China; hthuang@126.com (H.H.); hwt918seed@126.com (W.H.); zixiang330@163.com (X.Z.); wangxiaomeng@njau.edu.cn (X.W.); jrliang@njau.edu.cn (J.L.)

[2] College of Environmental Science and Engineering, Guilin University of Technology, Guilin 541004, China

* Correspondence: lxzhou@njau.edu.cn; Tel.: +86-13805184813

Abstract: The effects of nitrogen sources on the biosynthesis of jarosite were investigated by analyzing the changes in pH, Fe^{2+}, total Fe (TFe), and jarosite production in a 9K culture medium containing different nitrogen sources. Three nitrogen sources, namely $(NH_4)_2SO_4$, carbamide ($CO(NH_2)_2$), and NH_4NO_3, were used in this study. The solution's pH and Fe^{2+} concentrations were set to 2.5 and 160 mmol/L, respectively. The results demonstrated that the three different nitrogen sources could be used by *Acidithiobacillus ferrooxidans* (*A. ferrooxidans*) LX5, but the degree of utilization differed. The addition of $(NH_4)_2SO_4$ facilitated the growth of *A. ferrooxidans* LX5 compared with the other two nitrogen sources, while the bacterial activity in the $CO(NH_2)_2$ set was minimum. The pH of the solution had an inverse correlation with bacterial activity. The mineralization rate using $(NH_4)_2SO_4$ as the nitrogen source was 42.48%, which was slightly higher than the rates obtained with $CO(NH_2)_2$ and NH_4NO_3 (31.67% and 35.35%, respectively). The resulting minerals showed a different appearance and chemical composition. However, the XRD spectra showed similar chemical structure. The jarosites were identified as a mixture of jarosite, ammonioiarosite, and carphosiderite.

Keywords: *Acidithiobacillus ferrooxidans*; nitrogen sources; jarosite; biological mineralization

check for updates

Citation: Huang, H.; Hu, W.; Zi, X.; Wang, X.; Liang, J.; Zhou, L. Effects of Different Nitrogen Sources on the Formation of Biogenic Jarosite. *Sustainability* **2023**, *15*, 15765. https://doi.org/10.3390/su152215765

Academic Editor: Giovanni Esposito

Received: 29 August 2023
Revised: 27 October 2023
Accepted: 3 November 2023
Published: 9 November 2023

1. Introduction

Acid mine drainage (AMD) is acidic wastewater formed via biochemical reactions during the mining process, primarily from sulfide minerals, such as pyrite. It contains significant amounts of Fe^{2+}, Fe^{3+}, SO_4^{2-}, and heavy metals with a pH of 2–6 [1,2]. Under low pH (<4.0) conditions, the oxidation of Fe^{2+} by atmospheric O_2 is hampered in AMD environments [3]. If AMD is discharged without proper treatment, it can result in contamination of water and soil, thereby endangering the health of animals, plants, and humans [4,5]. Major mining countries, such as China, the United States, Canada, and Spain face challenges due to AMD. Approximately 20,000 to 50,000 mines worldwide generate AMD, and nearly 19,300 km^2 of fresh water and 720 km^2 of lakes and reservoirs are polluted by AMD [6]. Extreme leachates were generated in the abandoned Tharsis mine in Spain, reaching even negative pH and concentrations of up to 194 g/L of Fe [7]. Leaching of reaction products into surface waters pollute more than 20,000 km of streams in the United States alone [5].

Currently, various AMD control and treatment technologies play an important role in reducing AMD synthesis, decreasing AMD acidity, and eliminating metal pollution. The treatment of AMD is accomplished via neutralization, microbial techniques, constructed wetlands, and membrane methods [8]. The microbial method primarily entails the use of sulfate-reducing bacteria (SRB) for dissimilatory sulfate reduction, resulting in the formation of insoluble metal sulfide precipitates by reacting S^{2-} with Cu^{2+}, Fe^{2+}/Fe^{3+}, Cd^{2+}, and other heavy metal ions present in water, resulting in a heavy metal removal rate exceeding 90% [9]. The simultaneous production of alkaline substances alleviates the acidity of

AMD [10,11]. The SBR treatment of AMD requires minimal technical investment and low operational expenses. However, the high acidity of AMD significantly hampers the growth of sulfate-reducing bacteria, thereby adversely affecting the bioreactor performance [12]. The constructed wetland system offers several advantages over physical and chemical processes, due to its cost-effectiveness, ease of operation and maintenance, and low energy requirements [13]. Its removal rate of heavy metals is 97% [14]. However, the inherent limitations of constructed wetlands include the need for extensive land, prolonged treatment, and significant environmental impact [15]. Certain plants exhibit limited tolerance to excessive levels of heavy metals, which can lead to plant death and subsequent damage of the wetland system. Membrane separation techniques including nanofiltration, ultrafiltration, electrodialysis, reverse osmosis, and membrane distillation are widely utilized to treat AMD. Membrane separation technology facilitates selective metal ion separation and recovery, sludge reduction, and high-quality water recycling. However, the membrane separation technology is suitable for stable acid media and can cause rapid and serious membrane pollution [16].

Chemical neutralization and its modification are widely used to ensure high efficiency and stability, with a utilization rate higher than 90%. However, when AMD is enriched with Fe^{2+}, $CaCO_3$ and $Ca(OH)_2$ are used to increase the pH of AMD [17,18]. The resulting hydroxide precipitate is unstable and susceptible to pH. Due to the formation of H_2CO_3, the solution pH increases to approximately 6 when $CaCO_3$ is used for neutralization [19], resulting in poor Fe^{2+} removal efficiency. Non-biological oxidation is a challenge at a pH below 5; however, biological oxidation can be carried out [20]. *A. ferrooxidans* is used to carry out microbial oxidation of AMD to generate secondary iron minerals, which can effectively remove iron and other heavy metals from wastewater, reducing the load for subsequent lime neutralization. Iron and heavy metals can be removed under lower pH conditions, resulting in a significant reduction in lime consumption. Accordingly, the resulting precipitation has limited potential risk for the environment.

The secondary mineral formation is important for the removal of Fe^{2+}, Fe^{3+}, and SO_4^{2-} in AMD, which is of great significance. Numerous studies have demonstrated that the secondary minerals induce heavy metal adsorption and precipitation [21,22]. *A. ferrooxidans* in AMD mediates the oxidation of Fe^{2+} to Fe^{3+}, which is then hydrolyzed to produce secondary minerals, such as jarosite (K, Na, NH_4, H_3O) $Fe_3(SO_4)_2(OH)_6$ and schwertmannite ($Fe_8O_8(OH)_6(SO_4)_4$). Schwertmannite contains hydroxyl and sulfate groups, and has a large specific surface area [23]. Jarosite is an uncommon and valuable yellow ocher inorganic pigment [24]. The adsorption capacity of schwertmannite for As can reach 120 mg/g [25] and 55 mg/g for Cr [26]. Cu^{2+} and Pb^{2+} exist on the surface of schwertmannite in the form of ternary complexes [27], which play an important role in the migration of heavy metals. In other studies, organic carbon was used to modify Fe_3O_4/schwertmannite (Fe_3O_4/Sch/OC) by introducing Fe_3O_4 into the *A. ferrooxidans*-driven Fe^{2+} oxidation to generate catalysts. Further, the in situ H_2O_2 was disintegrated to produce •OH in a Fe_3O_4/Sch/OC-driven Fenton reaction to degrade the methylene blue (MB) [28]. Several parameters, including temperature, pH, crystal species, Fe^{2+} concentration, and monovalent cation, affect *A. ferrooxidans*-induced Fe^{2+} oxidation and the formation of secondary iron minerals [29,30]. Monovalent cations have a strong alum-forming ability, in the order of $K^+ > NH_4^+ > Na^+$ [25]. Further, K^+ promotes the oxidation of Fe^{2+} by *A. ferrooxidans*.

A. ferrooxidans, which is present in AMD, oxidizes Fe^{2+} and reduces sulfur compounds to generate metabolic energy. It has been used in AMD treatment, biological hydrometallurgy, and desulfurization [31]. *A. ferrooxidans* is an obligate aerobic Gram-negative electrochemical autotroph, which utilizes reduced pentose phosphate cycle (Calvin–Benson cycle) to immobilize CO_2 as the sole carbon source for growth [32]. The oxidation of Fe^{2+} by *A. ferrooxidans* is mainly controlled by the electron transport chain [33]. Cyc2 in the outer membrane of *A. ferrooxidans* is the key protein mediating electron transfer between extracellular inorganic iron and the intracellular metabolism [34]. Microorganisms require external carbon sources to initiate growth. These carbon sources are converted into different

metabolic intermediates, such as pyruvate and oxaloacetic acid, through various metabolic pathways. Amino acids are then synthesized using sources of nitrogen and sulfur, and other elements. Finally, proteins are synthesized by ribosomes. Nitrogen is an important component of biomolecules, such as amino acids, pyrimidines, purines, and enzyme cofactors. Therefore, when nitrogen is deficient, amino acid synthesis is severely affected [35], thereby hindering the oxidative activity of *A. ferrooxidans*. Bacteria absorb a variety of nitrogen sources as well as specific nitrogen compounds to maintain growth [36]. Studies have shown that *A. ferrooxidans* uses specific amino acids as nitrogen sources. However, the strain exhibited a lower growth rate and a growth yield when compared with a medium containing Fe^{2+}-NH_4^+-salts, which suggested that the ammonium ion was a superior nitrogen source compared with amino acids [37]. The nutrient solution for *A. ferrooxidans* LX5 growth traditionally contains 9K medium carrying $(NH_4)_2SO_4$ as a nitrogen source. Currently, the effect of nitrogen sources on biological mineralization mediated by *A. ferrooxidans* LX5 has received minimum attention. In contrast, several relevant studies have focused on the desulfuration of *Thiobacillus ferrooxidans* under different nutritional conditions [31]. Briceo and Tuovinen et al. [38,39] analyzed the impact of culture composition on bacterial growth and the subsequent precipitation by modifying the composition of the 9K medium used to cultivate *T. ferrooxidans*. Zhang et al. [40] decreased the concentrations of NH_4^+ and K^+ in the nutrient medium by replacing the sources of nitrogen ($(NH_4)_2SO_4$) and phosphorus (K_2HPO_4) with $(NH_4)_2HPO_4$, which not only maintained a high oxidative activity for bacterial growth but also reduced the yield of the mineral precipitate.

After pre-oxidizing Fe^{2+} to Fe^{3+}, the Fe^{2+}-rich AMD can be effectively neutralized under low pH conditions using inexpensive limestone. The resulting sediment exhibits excellent settling performance, with a low water content, and minimal volume. Therefore, the "Fe^{2+} bio-oxidation-neutralization" can be used to effectively treat AMD containing significant levels of Fe, especially Fe^{2+}. However, the low rate of Fe^{2+} bio-oxidation is a challenge. Additionally, during the Fe pre-oxidation stage, only *A. ferrooxidans* is utilized to oxidize Fe^{2+} to Fe^{3+} in AMD, without removing soluble iron from the water. It does not reduce the load of subsequent neutralization. Development of an efficient Fe^{2+} bio-oxidation method is therefore crucial to decrease the load on the lime neutralization, minimize the usage of neutralizers and sludge generation for Fe^{2+} removal from AMD, and ultimately decrease the cost associated with subsequent neutralization. In actual water processing, the treatment efficiency is improved by altering the type of nitrogen sources. The current investigation maximized the removal of soluble iron in AMD via precipitation of jarosite. This process involved the oxidation of Fe^{2+} and subsequent hydrolysis of Fe^{3+} mediated by *A. ferrooxidans* LX5. Thus, the effect of nitrogen sources on the jarosites generated via Fe^{2+} oxidization and Fe^{3+} hydrolysis by *A. ferrooxidans* LX5 was investigated. The findings are expected to facilitate practical engineering applications.

2. Materials and Methods

2.1. Concentrated Solution of A. ferrooxidans LX5 and Nitrogen-Free 9K Solution

The laboratory isolates of *A. ferrooxidans* LX5 are currently stored in the China General Microbiological Culture Collection Center under the preservation number CGMCC No. 0727.

A. ferrooxidans LX5 was inoculated in 9K medium composed of 44.24 g of $FeSO_4 \cdot 7H_2O$, 3.0 g of $(NH_4)_2SO_4$, 0.50 g of K_2HPO_4, 0.50 g of $MgSO_4 \cdot 7H_2O$, 0.10 g of KCl, and 0.01 g of $Ca(NO_3)_2 \cdot 4H_2O$ in the presence of 1 L of deionized water. The pH was adjusted to 2.5 using 9 M H_2SO_4 in a volume ratio (v/v) of 10%. The total volume of the reaction system was 250 mL. The reaction was performed at 28 °C and 180 rpm. In the late stage of the exponential growth phase (about 3 d) [29], the nutrient solution was filtered through a qualitative filter paper to remove the resulting iron precipitate. The bacterial density in the filtrate was found to be approximately 6×10^7 cells/mL, based on a double-plate method [29]. The filtered bacterial solution was further centrifuged at 10,000× g and 4 °C for 10 min to obtain the thallus. The thallus obtained was rinsed three times with a diluted

H_2SO_4 solution (with an approximate pH of 1.5) to eliminate various hetero ions. The bacterial solution derived from the 250 mL culture system was suspended in 5 mL of an acidic solution (pH 2.5) generated by adding H_2SO_4 with the concentration ratio set to 50. The resulting solution represented concentrated *A. ferrooxidans* LX5 solution.

The nitrogen-free 9K solution was prepared by dissolving 10.0 g of K_2HPO_4, 10.0 g of $MgSO_4 \cdot 7H_2O$, 2.0 g of KCl, and 0.2 g of $CaCl_2 \cdot 6H_2O$ ($CaCl_2 \cdot 6H_2O$ was used to replace $Ca(NO_3)_2 \cdot 4H_2O$) in 1 L of deionized water. The pH of the solution was adjusted to 2.5 by adding an equal volume of H_2SO_4 for used in the follow-up tests.

2.2. Effects of Nitrogen Sources on the Mineralization of A. ferrooxidans LX5

A single test involved three treatments, and each treatment was performed in triplicate. A 12.5 mL aliquot of nitrogen-free 9K medium was added to a 500 mL conical bottle. The nitrogen sources were $(NH_4)_2SO_4$, carbamide ($CO(NH_2)_2$), and NH_4NO_3. The dose of nitrogen in each treatment was 1 g. The concentrations of nitrogen source in the reaction system were 61, 133, and 50 mmol/L, respectively. The initial concentration of Fe^{2+} was set to match the concentration used in previous bacterial cultures based on 9K medium The Fe^{2+} was traced to $FeSO_4 \cdot 7H_2O$ (11.06 g), and its concentration was 160 mmol/L (8960 mg/L). Each treatment was inoculated with 1 mL of the concentrated bacterial solution. A controlled pH (range: 2.0–2.5) was recommended to facilitate the conversion of secondary iron minerals into jarosite and enhance the precipitation of total iron (TFe) [41]. Therefore, in this experiment, an initial pH of 2.5 was set. The total volume of the reaction system was 250 mL, and the culture was vortexed at 28 °C and 180 rpm.

During the entire culture, the pH of the solution was monitored regularly. The concentrations of Fe^{2+} and total iron were analyzed after filtration through a 0.22 μm membrane. The samples were collected at 6 h, 12 h, 24 h, 48 h, 72 h, and 96 h. The mineral precipitates were collected at the end of the culture using qualitative filter paper. These mineral sediments were washed twice with deionized water (pH 1.5) and twice with deionized water. Next, they were dried to a constant weight at 60 °C before being stored in a vacuum drying chamber. The elemental composition of these minerals was evaluated after acid dissolution.

The purpose of pre-oxidation of Fe^{2+}-rich AMD is to oxidize Fe^{2+} to Fe^{3+} and remove a portion of the soluble iron from the water, thus decreasing the load of subsequent neutralization reaction, reducing the amount of neutralizer used, and the amount of sludge generated. Iron can be completely removed via "Fe^{2+} biological oxidation-neutralization". Extension of the reaction indeed enhanced the rate of iron removal. However, the increase is relatively small and is related to the rate of Fe^{3+} hydrolysis. Complete oxidation of Fe^{2+} also attenuates the rate of Fe^{3+} hydrolytic mineralization. Therefore, in this experiment, the experiment was terminated at 96 h when all the Fe^{2+} in the three systems was completely oxidized.

2.3. Analytical Methods

The solution pH was tested with a pHS-3C acidity meter (Shanghai Leici Factory, Shanghai, China). Fe^{2+} was measured using the phenanthroline colorimetric method. The TFe test entailed initial reduction of Fe^{3+} to Fe^{2+} with hydroxylamine hydrochlorides, followed by phenanthroline colorimetry. The weight of minerals was recorded using an electronic scale (China Bailing, Xuzhou, China).

The TFe precipitation rate was determined as follows:

$$TFe\ (\%) = (TFe_{initial} - TFe_t)/TFe_{initial} \times 100,$$

where $TFe_{initial}$ represents the initial iron concentration, and TFe_t is the iron concentration at t (hours) of reaction time.

The oxidation rate of Fe^{2+} was calculated as:

$$Fe^{2+}\ (\%) = \left(Fe^{2+}_{initial} - Fe^{2+}_t\right)/Fe^{2+}_{initial} \times 100,$$

where $Fe^{2+}_{initial}$ denotes the initial Fe^{2+} concentration, and Fe^{2+}_{t} is the Fe^{2+} concentration at t (hours) of reaction time.

In the same experiment, three sets of parallel samples were utilized to obtain error bars.

The mineral phases of the sediments were identified using an X-ray diffractometer (XRD, X'Pert PRO, Panaco, Almelo, The Netherlands) under the following conditions: tube voltage, 50 kV; tube current, 150 mA; scanning interval, 10–80° (2θ); step length, 0.02°; scan rate, 5°/min; and Cu target (curved-crystal monochromator).

The morphology of the sediments was analyzed using a Hitachi S-4800 scanning electron microscope (Tokyo, Japan). Samples were pasted onto the working table with a double sticky tape and then coated with a 10 nm gold film using an ion-sputtering instrument. The samples were observed under an accelerating voltage of 3.0 kV.

The elemental analysis of the secondary minerals was performed using a portable ore analyzer (Innov-X Explorer-9000SDD, Enos, Schaumburg, IL, USA). The samples were tested under two modes (soil and two-beam ore), with assistance from the Guangxi Key Laboratory of Environmental Pollution Control Theory and Technology, Guilin University of Technology.

Microsoft Excel® 2019 was used to determine the mean and standard deviation of each data point. All figures were drawn using Origin® 9.0 software.

3. Results and Discussion

3.1. Change in the pH of a Solution during the Reaction with Different Nitrogen Sources

The pH changes in the reaction systems containing different sources of nitrogen are shown in Figure 1.

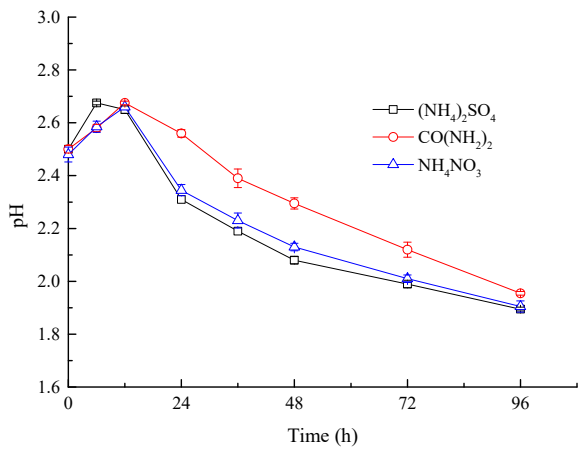

Figure 1. Variation in solution pH during 96 h of culture in the presence of different nitrogen sources.

The variation in pH was consistent in the presence of different sources of nitrogen. The pH of the solution initially increased and subsequently decreased as the culture time was prolonged [42]. Fe^{2+} oxidation in the bacteria accompanied by H^+ consumption increased the pH of the solution. Subsequently, the Fe^{3+} ions generated continuously were hydrolyzed to release H^+ and slightly lower the pH of the solution. This phenomenon was consistent with our previous study [43], which demonstrated that *A. ferrooxidans*-mediated biological mineralization entailed initial acid consumption, followed by acid production. However, no clear boundary was detected, and the change in pH was a comprehensive manifestation of the following reaction mechanism:

① Oxidation of Fe^{2+} to Fe^{3+} involving consumption of H^+.

$$4Fe^{2+} + O_2 + H^+ \xrightarrow{A.\ ferrooxidans} 4Fe^{3+} + 2H_2O \quad (1)$$

② Hydrolysis of Fe^{3+} to schwertmannite or jarosites and release of H^+.

$$Fe^{3+} + SO_4^{2-} + 14H_2O \rightarrow Fe_8O_8(OH)_6(SO_4)_4(\text{schwertmannite}) + 22H^+ \quad (2)$$

$$M + 3Fe^{3+} + 2SO_4^{2-} + 6H_2O \rightarrow MFe_3(SO_4)_2(OH)_6(\text{jarosites}) + 6H^+ M = \left(NH_4^+, K^+, H_3O^+\right) \quad (3)$$

The addition of $(NH_4)_2SO_4$ increased the pH of the system during the first 6 h, followed by a decline. The pH of the other two reaction systems showed an upward trend within 12 h. However, the pH of the carbamide system was slightly higher, which might be attributed to the products of alkaline hydrolysis. The pH of the carbamide system after 12 h of reaction was higher than that of $(NH_4)_2SO_4$, which was consistent with the results of a previous study [44]. After 12 h, the solution pH started to decline rapidly due to the steady consumption of NH_4^+ by the bacteria. After 96 h of reaction duration, the $(NH_4)_2SO_4$, carbamide, and NH_4NO_3 reaction systems had pH values of 1.90, 1.96, and 1.90, respectively. The pH of the carbamide system was the highest during the entire reaction, while the pH of the $(NH_4)_2SO_4$ system was the least. The reaction steps (2) and (3) indicate that 1 mol of Fe^{3+} was hydrolyzed to produce 2.75 mol H^+ of schwertmannite, and 2 mol of H^+ of jarosites was released. Fe^{3+} was hydrolyzed in the solution, which decreased the levels of Fe^{3+} and pH. The findings suggest that an increase in the production of secondary minerals led to a corresponding increase in the synthesis of H^+, resulting in a decrease in pH. This observation was consistent with the rate of TFe precipitation. Further, the highest yield of secondary minerals was obtained using $(NH_4)_2SO_4$ as a nitrogen source.

3.2. Effects of Nitrogen Source on Fe^{2+} Oxidization

The oxidation of Fe^{2+} in different reaction systems is shown in Figure 2. The average oxidation rate of Fe^{2+} was used for quantitative comparison, based on that shown in Table 1.

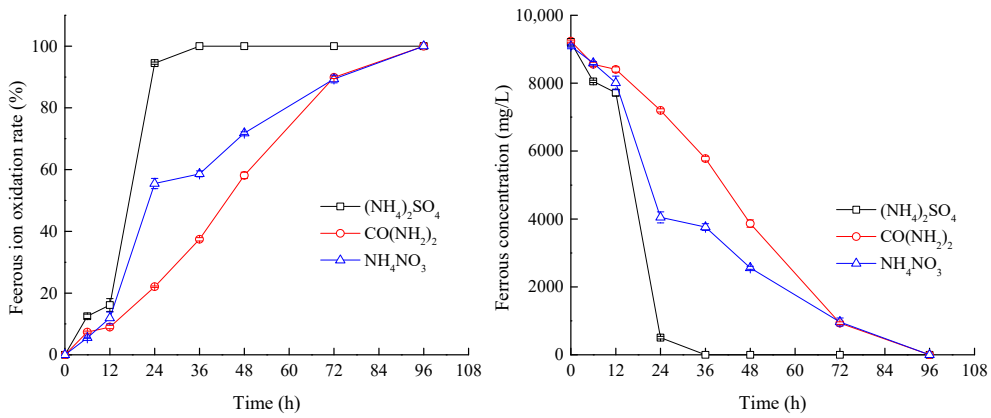

Figure 2. Effects of different nitrogen sources on Fe^{2+} oxidation.

Table 1. Effects of different nitrogen sources on the mean rate of Fe^{2+} oxidation (mg/(L·h)).

Time (h)	Nitrogen		
	$(NH_4)_2SO_4$	$CO(NH_2)_2$	NH_4NO_3
0–12	124	69	90
12–24	601	100	330
24–36	42	118	24
36–72	-	135	78
72–96	-	39	40

The oxidation efficiency of Fe^{2+} in all the reaction systems was relatively low (<20%) within the initial 12 h. In particular, the oxidation rate of Fe^{2+} was only 9.02% in the car-

bamide reaction system. Compared with the reaction duration of 12 h to 24 h, the average speed of oxidation within the initial 6 h was less than 150 mg/(L·h), indicating relatively slow oxidation. The average oxidation speed was only 69 mg/(L·h) in the carbamide reaction system. At 24 h, the oxidation rate of Fe^{2+} in the $(NH_4)_2SO_4$ reaction system rapidly increased to 94.49%, and the oxidation speed was significantly elevated to 601 mg/(L·h). The oxidation rates of Fe^{2+} in the carbamide and NH_4NO_3 reaction systems were 22.07% and 55.50%, respectively, corresponding to oxidation speeds of 100 mg/(L·h) and 330 mg/(L·h), respectively. These values were substantially lower than in the $(NH_4)_2SO_4$ reaction system. The Fe^{2+} was completely oxidized to Fe^{3+} in the $(NH_4)_2SO_4$ reaction system after 36 h, while only 37.43% and 50.63% of Fe^{2+} ions were converted in the carbamide and NH_4NO_3 reaction systems, respectively. The Fe^{2+} ions in the carbamide and NH_4NO_3 reaction systems were oxidized completely until 96 h. The oxidation efficiency of Fe^{2+} directly reflected bacterial activity. The higher oxidation speed corresponded to a greater oxidation rate and stronger activity of *A. ferrooxidans* [45]. The nitrogen (N) levels in $(NH_4)_2SO_4$, $CO(NH_2)_2$, and NH_4NO_3 were 21.2%, 46.6%, and 35.0%, respectively. Therefore, carbamide had the highest available N content, and $(NH_4)_2SO_4$ showed the least available N level when the same mass of nitrogen sources was fed to *A. ferrooxidans*. However, the oxidation speed of Fe^{2+} was the highest in the $(NH_4)_2SO_4$ reaction system and the least in the NH_4NO_3 reaction system. This result indicates that the three nitrogen sources were utilized by *A. ferrooxidans* LX5 to different degrees. Previous studies demonstrated [44] that *A. ferrooxidans* induced the hydrolysis of carbamide. Carbamide was mainly synthesized from cell metabolism, and it generated CO_2 except for the available N. This mechanism facilitated cell metabolism. However, *A. ferrooxidans* is a chemoheterotroph that obtains energy for bacterial growth by oxidizing Fe^{2+} to Fe^{3+}. The hydrolysis of carbamide turns the solution alkaline. The OH^- released combines with soluble iron, resulting in precipitation. The oxidation speed of Fe^{2+} was gradually retarded as the source of energy was consumed by *A. ferrooxidans*. The growth of *A. ferrooxidans* was affected by anions in the solution, which further controlled the oxidation capacity of Fe^{2+}. Anions affected the activity of *A. ferrooxidans* in the following order: $NO_3^- > Cl^- > SO_4^{2-}$ [46]. Thus, SO_4^{2-} has minimal effect on the growth of *A. ferrooxidans*, while Cl^- and NO_3^- levels inhibit bacterial activity. The presence of NO_3^- strongly suppressed bacterial growth and potentially led to bacterial mortality. The high NO_3^- concentrations (49.4–65.8 mmol/L) inhibited Fe^{2+} bio-oxidation during the initial stage [47]. Further, the Fe^{2+} bio-oxidation capacity of *A. ferrooxidans* was inhibited by treatment with 8.2–65.8 mg/L NO_3^-. In this experiment, NH_4NO_3 was utilized as a nitrogen source, with an initial NO_3^- concentration of 50 mmol/L. The findings indicate that the activity of *A. ferrooxidans* was inhibited, which was consistent with the previous study findings [47]. Consequently, the addition of NH_4NO_3 as a nitrogen source suppressed *A. ferrooxidans* LX5 growth and subsequently reduced bacterial activity. As SO_4^{2-} is one of the metabolites, *A. ferrooxidans* can tolerate a high concentration of SO_4^{2-}. Studies have also reported that SO_4^{2-} facilitate the electron transport of copper atoms from an iron–sulfur cluster to ceruloplasmin in an oxygen-dependent electron transport chain. Further, in vitro studies of iron and ceruloplasmin oxidoreductase revealed that ceruloplasmin was only reduced by ferrous ions in the presence of sulfate ions [48].

The utilization of the three nitrogen sources differed during the mineralization of *A. ferrooxidans* LX5. In general, *A. ferrooxidans* LX5 prefers the $(NH_4)_2SO_4$ reaction system, followed by the NH_4NO_3 system and the carbamide reaction system.

3.3. Effects of Nitrogen Sources on Mineralization Efficiency

The changes in soluble iron levels in the different reaction systems are depicted in Figure 3. Further, the hydrolysis of Fe^{3+} induced a partial phase transition of iron from liquid to solid via synthesis of jarosite [49].

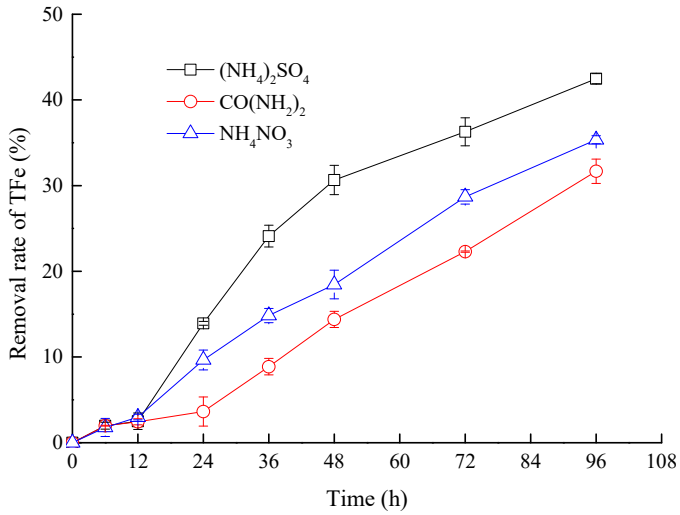

Figure 3. Effects of different nitrogen sources on the removal of total iron.

As shown in Figure 3, the precipitation rate of TFe showed no significant difference in the three reaction systems within the initial 12 h, which was only about 2.45–2.99%. However, the precipitation rate differed increasingly after 12 h. The precipitation rate of TFe in the $(NH_4)_2SO_4$ reaction system was significantly higher than in the carbamide and NH_4NO_3 reaction systems. The precipitation rate of TFe in the $(NH_4)_2SO_4$ reaction system was the highest (42.48%) at 96 h, followed by the NH_4NO_3 (35.35%) and carbamide reaction systems (31.67%). The rate of Fe^{3+} hydrolytic mineralization is directly proportional to the rate of Fe^{3+} supply. A higher rate of Fe^{3+} supply accelerated the formation of secondary minerals and increased the precipitation of TFe [50]. However, the rate of Fe^{3+} hydrolytic mineralization slows down once Fe^{2+} is completely oxidized. Based on the analysis of Fe^{2+} oxidation rate, it can be concluded that the treatment utilizing $(NH_4)_2SO_4$ as a nitrogen source rapidly generated Fe^{3+}, thereby promoting the formation of secondary minerals, resulting in maximum TFe precipitation. Thus, nitrogen sources control mineralization efficiency. $(NH_4)_2SO_4$ was the most efficient nitrogen source for the mineralization of *A. ferrooxidans* LX5.

The weights of jarosite based on different reaction systems after 96 h are presented in Figure 4.

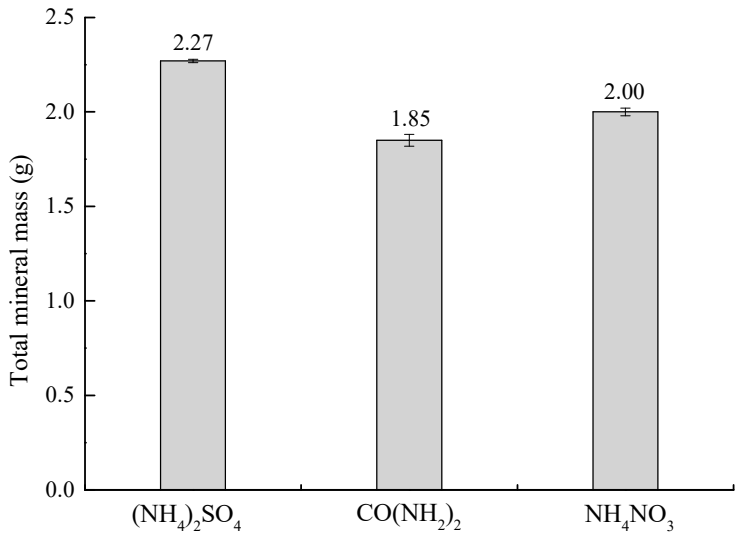

Figure 4. The total mass of minerals generated by different nitrogen source reaction systems.

The mineral mass showed a positive correlation with the efficiency of TFe precipitation. The mineral masses of $(NH_4)_2SO_4$, carbamide, and NH_4NO_3 reaction systems were 2.27 g, 1.85 g, and 2.00 g, respectively. The conversion rates of iron from solution to minerals were 42.48%, 31.67%, and 35.35% in the $(NH_4)_2SO_4$, carbamide, and NH_4NO_3 reaction systems, respectively, based on the changes in initial and final iron concentrations.

3.4. Identification and Analysis of Sediments

3.4.1. XRD and Chemical Element Analysis

X-ray diffraction (XRD) is the most common method used to identify the mineral phases, as it can distinguish different categories of crystalline minerals from amorphous structures [51]. The XRD spectra of different mineral sediments (Figure 5) show that the minerals formed in different reaction systems exhibited consistent peaks. The location of the highest diffraction peak remained constant within an error in the range of ±0.2°. The main diffraction peak attributed to $(NH_4)_2SO_4$ and NH_4NO_3 was slightly higher than that of carbamide, and the crystallinity of the mineral phase increased slightly. Secondary minerals containing high levels of iron including jarosites and schwertmannite often co-existed during the test. Schwertmannite, an amorphous mineral, exhibits a broad characteristic peak [52]. Based on the standard spectrum of schwertmannite (PDF#047-1775), the characteristic peak of schwertmannite was identified at $2\theta = 35.16°$ [53], which was not significant. The comparative analysis revealed mineral sediments as mixtures of $KFe_3(SO_4)_2(OH)_6$, $NH_4Fe_3(SO_4)_2(OH)_6$, and $H_3OFe_3(SO_4)_2(OH)_6$.

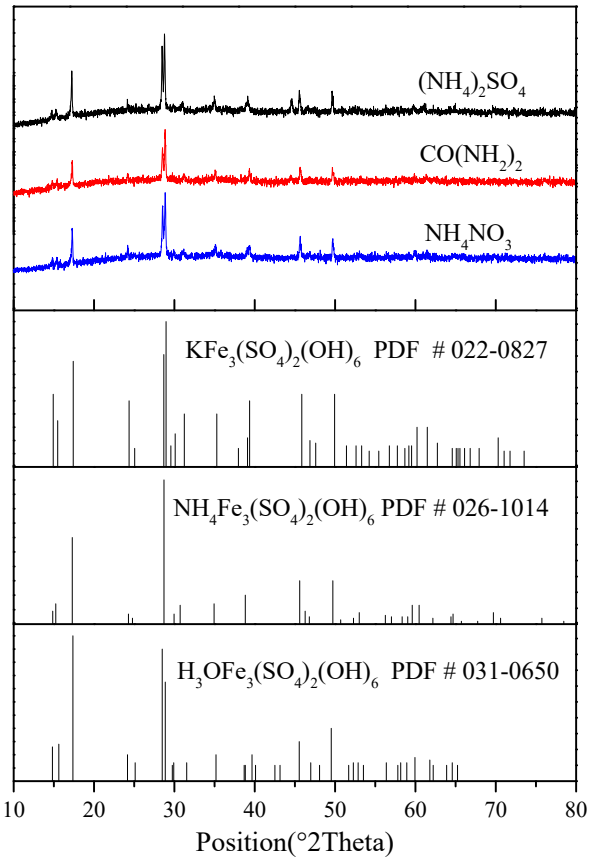

Figure 5. XRD patterns of precipitates obtained from different nitrogen sources.

The chemical composition of the mineral precipitates (Table 2) showed significant differences in iron content. The iron levels in the minerals obtained from $(NH_4)_2SO_4$, carbamide, and NH_4NO_3 systems were 32.8%, 20.9%, and 28.6%, respectively. The iron content in the mineral formed from $(NH_4)_2SO_4$ reaction system was comparable to the theoretical value. The iron levels in jarosite, ammonioiarosite, and carphosiderite were

33.5%, 35.0%, and 34.8%, respectively. However, the iron levels in the other two systems were slightly lower than the theoretical values. In particular, the iron content in the jarosite derived from the carbamide-containing system was 12.6%, which was substantially less than the theoretical value. In addition, the K, N, and SO_4^{2-} levels were relatively low in all the minerals obtained. The K and N ratios were significantly lower than those of ideal minerals. The short reaction time (96 h) in this experiment may be a contributing factor, as extending the reaction time appropriately enhanced the levels of monovalent cations in synthetic minerals [54]. Higher levels of Fe^{3+} during the initial stage of the reaction induced the formation of crystalline jarosite [55]. Combined with the above Fe^{2+} oxidation rate, the oxidation rates of $(NH_4)_2SO_4$ and NH_4NO_3 were substantially higher than that of carbamide in the first 24 h of the reaction, which facilitated the formation of crystalline jarosite. The substitution of monovalent cations by H_3O^+ in jarosite is a widely recognized phenomenon. Therefore, the iron precipitates in these tests represent mixtures of jarosite, ammonioiarosite, and carphosiderite.

Table 2. Elemental analyses of precipitates derived from different nitrogen sources.

Nitrogen	K (wt.%)	N (wt.%)	Fe (wt.%)	SO_4^{2-} (wt.%)
$(NH_4)_2SO_4$	1.10	0.22	32.8	21.6
$CO(NH_2)_2$	1.79	0.35	20.9	22.3
NH_4NO_3	1.43	0.18	28.6	21.0
$KFe_3(SO_4)_2(OH)_6$	7.80		33.5	38.3
$NH_4Fe_3(SO_4)_2(OH)_6$		2.92	35.0	40.0
$H_3OFe_3(SO_4)_2(OH)_6$			34.8	40.0

3.4.2. SEM Analysis

The SEM images of jarosite formed in different reaction systems are shown in Figures 6–8.

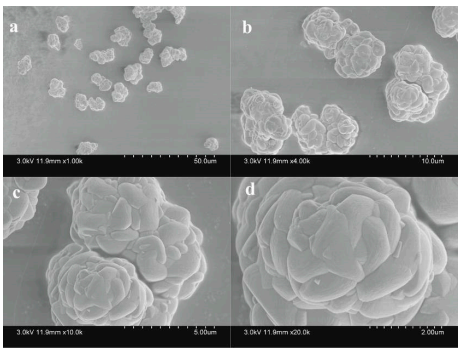

Figure 6. Scanning electron micrograph of jarosite generated using ammonium sulfate as a nitrogen source ((**a**) ×1000; (**b**) ×4000; (**c**) ×10,000; and (**d**) ×20,000).

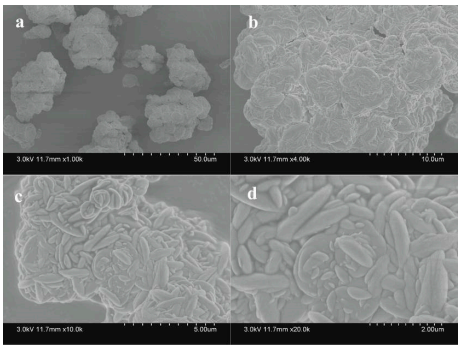

Figure 7. Scanning electron micrograph of jarosite derived from carbamide as a nitrogen source ((**a**) ×1000; (**b**) ×4000; (**c**) ×10,000; and (**d**) ×20,000).

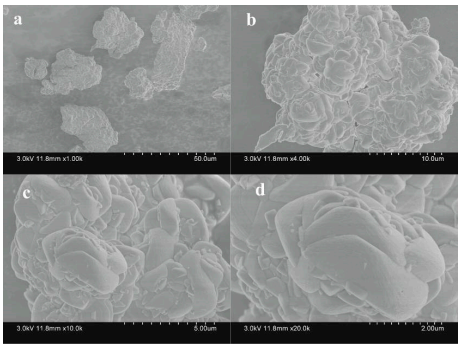

Figure 8. Scanning electron micrograph of jarosite obtained from ammonium nitrate as a nitrogen source ((**a**) ×1000; (**b**) ×4000; (**c**) ×10,000; and (**d**) ×20,000).

Jarosites are composed of multiple micron crystal clusters with approximate diameters ranging from 2 μm to 10 μm. They exhibit a smooth surface and clear profile. SEM images reveal similar morphology of minerals produced in the $(NH_4)_2SO_4$ and NH_4NO_3 reaction systems. The form cauliflower-like crystal clusters with smooth surfaces. The minerals produced in the carbamide reaction system exhibit smooth surfaces and clusters of irregular moon-shaped crystals. SEM analyses revealed slight variation in the morphology of minerals generated in different reaction systems. However, the peak positions of the XRD spectra were basically similar. Figures 6–8 do not show the typical structure of amorphous schwertmannite [56]. Schwertmannite is a metastable substance. Schwertmannite transforms into highly crystalline jarosite at a pH less than 3 in the presence of monovalent cations, such as K^+ and Na^+ [57]. This transformation is consistent with the results of XRD analysis mentioned earlier. Additionally, the minerals formed from different nitrogen sources are expected to be a mixture of jarosite, ammonioiarosite, and carphosiderite.

4. Conclusions

Currently, active treatment systems based on lime neutralization of acidity and precipitation of harmful elements are the most common methods used to treat AMD. However, most of the Fe in AMD exists as Fe^{2+}, suggesting the need for generation and removal of $Fe(OH)_2$ precipitate at a pH 8–9. This strategy not only requires increasing levels of lime but also produces treatment wastewater with high pH and hardness, which is detrimental to the environment. It also hinders hydroxide gel sedimentation. Therefore, introducing a Fe^{2+} bio-oxidation stage before the neutralization reaction by inoculating *A. ferrooxidans* can lead to rapid oxidation of Fe^{2+} to Fe^{3+} under low hydrolysis for secondary mineral precipitation. Dissolved Fe can be directly removed from AMD, while other harmful components are eliminated via adsorption and co-precipitation. Thereby, both the load on subsequent neutralization and the amount of generated sludge are decreased by minimizing the amount of neutralizer required. The objective of this study was to maximize soluble iron removal from AMD during the Fe^{2+} bio-oxidation stage via jarosite precipitation. To address the low bio-oxidation rates of Fe^{2+}, this study analyzed the effect of nitrogen source on the oxidation of Fe^{2+} by *A. ferrooxidans* LX5 and Fe^{3+} hydrolysis to generate jarosite. The study findings are summarized below:

(1) The pH of the solution was decreased by *A. ferrooxidans*. Carbamide supplementation yielded the highest pH value, followed by treatment with NH_4NO_3 and $(NH_4)_2SO_4$.
(2) The utilization efficiency of $(NH_4)_2SO_4$ was the highest, followed by NH_4NO_3. The microbial activity of *A. ferrooxidans* LX5 was the lowest in the $CO(NH_2)_2$-dosing reaction system. The rate of TFe precipitation in the $(NH_4)_2SO_4$-containing system was substantially higher than in the carbamide- and NH_4NO_4-containing systems. Compared with the other two nitrogen sources, $(NH_4)_2SO_4$ was strongly conducive to the growth of *A. ferrooxidans* LX5.

(3) The morphologies and chemical compositions of minerals varied slightly when different nitrogen sources were used. However, the peak positions on the XRD spectra were basically consistent. The resultant secondary mineral was a mixture of jarosite, ammonioiarosite, and carphosiderite.
(4) Using $(NH_4)_2SO_4$ as a nitrogen source, *A. ferrooxidans* LX5 oxidized Fe^{2+} to Fe^{3+} within 36 h at a low pH of 2.5. At the end of the 96 h experiment, approximately 42.48% of soluble Fe yielded secondary iron-containing minerals, which were effectively removed. The enhanced biological oxidation of Fe^{2+} compared with traditional neutralization technique has significant practical implications for lime neutralization. It minimizes the usage of neutralizers, and decreases sludge generation.

Author Contributions: Conceptualization, H.H. and L.Z.; methodology, H.H.; investigation, H.H. and W.H.; resources, X.Z. and J.L.; data curation, H.H. and W.H.; writing—original draft preparation, H.H.; validation, L.Z.; writing—review and editing, X.W.; funding acquisition, L.Z. All authors have read and agreed to the published version of the manuscript.

Funding: Research was supported by the National Natural Science Foundation of China (22336003).

Institutional Review Board Statement: Not applicable.

Informed Consent Statement: Not applicable.

Data Availability Statement: Data are contained within the article.

Conflicts of Interest: The authors declare no conflict of interest.

References

1. Rambabu, K.; Banat, F.; Pham, Q.M.; Ho, S.-H.; Ren, N.-Q.; Show, P.L. Biological Remediation of Acid Mine Drainage: Review of Past Trends and Current Outlook. *Environ. Sci. Ecotechnol.* **2020**, *2*, 100024. [CrossRef] [PubMed]
2. Jiao, Y.; Zhang, C.; Su, P.; Tang, Y.; Huang, Z.; Ma, T. A review of acid mine drainage: Formation mechanism, treatment technology, typical engineering cases and resource utilization. *Process Saf. Environ. Prot.* **2023**, *170*, 1240–1260. [CrossRef]
3. Yang, J.; Wang, R.; Wang, H.; Song, Y. The Important Role of Dissolved Oxygen Supply Regulated by the Hydraulic Shear Force during the Biosynthesis of Iron Hydroxysulfate Minerals. *Minerals* **2020**, *10*, 518. [CrossRef]
4. Sobron, P.; Rull, F.; Sobron, F.; Sanz, A.; Medina, J.; Nielsen, C. Raman spectroscopy of the system iron(III)–sulfuric acid–water: An approach to Tinto River's (Spain) hydrogeochemistry. *Spectrochim. Acta Part A Mol. Biomol. Spectrosc.* **2007**, *68*, 1138–1142. [CrossRef]
5. Skousen, J.G.; Ziemkiewicz, P.F.; McDonald, L.M. Acid mine drainage formation, control and treatment: Approaches and strategies. *Extr. Ind. Soc.* **2019**, *6*, 241–249. [CrossRef]
6. Yang, Y.; Li, B.; Li, T.; Liu, P.; Zhang, B.; Che, L. A review of treatment technologies for acid mine drainage and sustainability assessment. *J. Water Process Eng.* **2023**, *55*, 104213. [CrossRef]
7. Raúl, M.G.; Carlos, R.C.; Manuel, O.; Macías, F. Seasonal variability of extremely metal rich acid mine drainages from the Tharsis mines (SW Spain). *Environ. Pollut.* **2020**, *259*, 113829.
8. Tong, L.; Fan, R.; Yang, S.; Li, C. Development and Status of the Treatment Technology for Acid Mine Drainage. *Min. Metall. Explor.* **2020**, *38*, 315–327. [CrossRef]
9. Akinpelu, E.A.; Ntwampe, S.K.O.; Fosso-Kankeu, E.; Nchu, F.; Angadam, J.O. Performance of microbial community dominated by Bacillus spp. in acid mine drainage remediation systems: A focus on the high removal efficiency of SO_4^{2-}, Al^{3+}, Cd^{2+}, Cu^{2+}, Mn^{2+}, Pb^{2+}, and Sr^{2+}. *Heliyon* **2021**, *7*, e072412021. [CrossRef]
10. Srivastava, S.; Agrawal, S.B.; Mondal, M.K. A review on progress of heavy metal removal using adsorbents of microbial and plant origin. *Environ. Sci. Pollut. Res.* **2015**, *22*, 15386–15415. [CrossRef]
11. Magowo, W.E.; Sheridan, C.; Rumbold, K. Global Co-occurrence of Acid Mine Drainage and Organic Rich Industrial and Domestic Effluent: Biological sulfate reduction as a co-treatment-option. *J. Water Process Eng.* **2020**, *38*, 101650. [CrossRef]
12. Naidu, G.; Ryu, S.; Thiruvenkatachari, R.; Choi, Y.; Jeong, S.; Vigneswaran, S. A critical review on remediation, reuse, and resource recovery from acid mine drainage. *Environ. Pollut.* **2019**, *247*, 1110–1124. [CrossRef] [PubMed]
13. Daraz, U.; Li, Y.; Ahmad, I.; Iqbal, R.; Ditta, A. Remediation technologies for acid mine drainage: Recent trends and future perspectives. *Chemosphere* **2022**, *311*, 137089. [CrossRef] [PubMed]
14. Gersberg, R.; Elkins, B.; Lyon, S.; Goldman, C. Role of aquatic plants in wastewater treatment by artificial wetlands. *Pergamon* **1986**, *20*, 363–368. [CrossRef]
15. Singh, S.; Envelope, S.C.P. Impact of seasonal variation on the treatment response of constructed wetlands receiving acid mine drainage in a subtropical region. *J. Water Process Eng.* **2022**, *49*, 103182. [CrossRef]

16. López, G.O.; Cortina, J.L. Integration of membrane technologies to enhance the sustainability in the treatment of metal-containing acidic liquid wastes. An overview. *Sep. Purif. Technol.* **2021**, *265*, 118485. [CrossRef]
17. Kaur, G.; Couperthwaite, S.J.; Millar, G.J. Alternative neutralisation materials for acid mine drainage treatment. *J. Water Process Eng.* **2018**, *22*, 46–58. [CrossRef]
18. Lauren, B.; Bethany, K. Calcium carbonate in waste flooring for neutralization of acid rock drainage. *Mine Water Environ.* **2023**, *42*, 70–77.
19. Akeil, A.; Koldas, S. Acid mine drainage (AMD): Causes, treatment and case studies. *J. Clean. Prod.* **2006**, *14*, 1139–1145.
20. Meruane, G.; Vargas, T. Bacterial oxidation of ferrous iron by *Acidithiobacillus ferrooxidans* in the pH range 2.5–7.0. *Hydrometallurgy* **2003**, *71*, 149–158. [CrossRef]
21. Asta, M.P.; Cama, J.; Martínez, M.; Giménez, J. Arsenic removal by goethite and jarosite in acidic conditions and its environmental implications. *J. Hazard. Mater.* **2009**, *171*, 965–972. [CrossRef] [PubMed]
22. Drouet, C.; Baron, D.; Navrotsky, A. On the thermochemistry of the solid solution between jarosite and its chromate analog. *Am. Mineral.* **2015**, *88*, 1949–1954. [CrossRef]
23. Chen, M.; Lu, G.; Guo, C.; Yang, C.; Wu, J.; Huang, W.; Yee, N.; Dang, Z. Sulfate migration in a river affected by acid mine drainage from the Dabaoshan mining area, South China. *Chemosphere* **2015**, *119*, 734–743. [CrossRef] [PubMed]
24. Mastrotheodoros, G.P.; Beltsios, K.G. Pigments-Iron-based red, yellow, and brown ochres. *Archaeol. Anthropol. Sci.* **2022**, *14*, 35. [CrossRef]
25. Song, Y.; Wang, H.; Yang, J.; Cao, Y. Influence of Monovalent Cations on the Efficiency of Ferrous Ion Oxidation, Total Iron Precipitation, and Adsorptive Removal of Cr(VI) and As(III) in Simulated Acid Mine Drainage with Inoculation of *Acidithiobacillus ferrooxidans*. *Metals* **2018**, *8*, 596. [CrossRef]
26. Ulatowska, J.; Stala, Ł.; Polowczyk, I. Comparison of Cr(VI) Adsorption Using Synthetic Schwertmannite Obtained by Fe^{3+} Hydrolysis and Fe^{2+} Oxidation: Kinetics, Isotherms and Adsorption Mechanism. *Int. J. Mol. Sci.* **2021**, *22*, 8175. [CrossRef]
27. Gan, M.; Li, M.-M.; Zeng, J.; Liu, X.-X.; Zhu, J.-Y.; Hu, Y.-H.; Qiu, G.-Z. *Acidithiobacillus ferrooxidans* enhanced heavy metals immobilization efficiency in acidic aqueous system through bio-mediated coprecipitation. *Trans. Nonferrous Met. Soc. China* **2017**, *27*, 1156–1164. [CrossRef]
28. Li, T.; Wang, Z.; Zhang, Z.; Feng, K.; Liang, J.; Wang, D.; Zhou, L. Organic carbon modified Fe_3O_4/schwertmannite for heterogeneous Fenton reaction featuring synergistic in-situ H_2O_2 generation and activation. *Sep. Purif. Technol.* **2021**, *276*, 119344. [CrossRef]
29. Wang, M.; Liang, J.; Zhou, L. The formation of biogenic jarosite by *Acidithiobacillus ferrooxidans* in the presence of crystal seed and potassium. *J. Nanjing Agric. Univ.* **2013**, *36*, 97–102.
30. Eftekhari, N.; Kargar, M.; Zamin, F.; Rastakhiz, N.; Manafi, Z. A Review on Various Aspects of Jarosite and Its Utilization Potentials. *Ann. De Chim. Sci. Des Matériaux* **2020**, *44*, 43–52. [CrossRef]
31. Qin, S.; Liu, X.; Lu, M.; Li, D.; Feng, X.; Zhao, L. *Acidithiobacillus ferrooxidans* and mixed Acidophilic microbiota oxidation to remove sulphur impurity from iron concentrate. *Biochem. Eng. J.* **2022**, *187*, 108647. [CrossRef]
32. Appia-Ayme, C.; Quatrini, R.; Denis, Y.; Denizot, F.; Silver, S.; Roberto, F.; Veloso, F.; Valdés, J.; Cárdenas, J.P.; Esparza, M.; et al. Microarray and bioinformatic analyses suggest models for carbon metabolism in the autotroph *Acidithiobacillus ferrooxidans*. *Hydrometallurgy* **2006**, *83*, 273–280. [CrossRef]
33. Jiang, V.; Khare, S.D.; Banta, S. Computational Structure Prediction Provides a Plausible Mechanism for Electron Transfer by the Outer Membrane Protein Cyc2 from *Acidithiobacillus ferrooxidans*. *Protein Sci.* **2021**, *30*, 1640–1652. [CrossRef] [PubMed]
34. Peng, Z.; Liu, Z.; Jiang, Y.; Dong, Y.; Shi, L. In vivo interactions between Cyc2 and Rus as well as Rus and Cyc1 of *Acidithiobacillus ferrooxidans* during extracellular oxidization of ferrous iron. *Int. Biodeterior. Biodegrad.* **2022**, *173*, 105453. [CrossRef]
35. Zhu, M.L.; Pan, Y.G.; Dai, X.F. (p)ppGpp: The magic governor of bacterial growth economy. *Curr. Genet.* **2019**, *65*, 1121–1125. [CrossRef] [PubMed]
36. Lu, P.L.; Yang, H.; Ding, A.Q.; Li, C.; Lin, Q. Metabolic regulation of bacteria with limited carbon and nitrogen sources. *Acta Microbiol. Sin.* **2023**, *63*, 946–962.
37. Tsuyoshi, S.; Shinji, T.; Kyoko, F.; Yamaryo, K.; Inagaki, K.; Tano, T. Utilization of Amino Acids as a Sole Source of Nitrogen by Obligate Chemolithoautotroph *Thiobacillus ferrooxidans*. *Agric. Biol. Chem.* **1987**, *51*, 2229–2236.
38. Briceo, P.G.D.; Gerardo, A.C.P.; Marco, A.M.G. Early reprecipitation of sulfate salts in coal biodesulfurization processes using acidophilic chemolithotrophic bacteria. *World J. Microbiol. Biotechnol.* **2020**, *36*, 81.
39. Tuovinen, O.H.; Kelly, D.P. Biology of *Thiobacillus ferrooxidans* in relation to the microbiological leaching of sulphide ores. *Z. Allg. Mikrobiol.* **1972**, *12*, 311–346. [CrossRef]
40. Zhang, Y.; Zhang, C.C.; Gou, J.X.; Li, Y.; Yang, L. Study of the effects of culture condition on the growth of *Thiobacillus ferrooxidans* and the jarosite precipitates. *J. Saf. Environ.* **2012**, *12*, 28–31.
41. Song, Y.W.; Wang, H.R.; Liang, J.R.; Zhou, L.X. Effects of temperature and pH on the formation of biogenic Fe(III) hydroxysulfate precipitates. *Acta Sci. Circumstantiae* **2016**, *36*, 3683–3690.
42. Wang, H.R.; Yang, L.L.; Wang, R.; Yang, J.; Cao, X.Y.; Song, Y.W. Fe^{2+} oxidation and mineralization properties of *A. ferrooxidans* biofilm immobilized on three fillers. *Acta Sci. Circumstantiae* **2022**, *42*, 160–168.

43. Song, Y.; Yang, L.; Wang, H.; Sun, X.; Bai, S.; Wang, N.; Liang, J.; Zhou, L. The coupling reaction of Fe^{2+} bio-oxidation and resulting Fe^{3+} hydrolysis drastically improve the formation of iron hydroxysulfate minerals in AMD. *Environ. Technol.* **2019**, *42*, 2325–2334. [CrossRef] [PubMed]
44. Zhang, X.; Wang, S.L.; Ding, Y.; Tao, X.X. Influence factors on growth and metabolism of pyrite sulfur-removing bacteria. *Ind. Miner. Process.* **2005**, *10*, 9–12.
45. Wang, H.; Guo, Q.; Guo, Z.; Luo, H.; Li, H.; Yang, J.; Song, Y. Assessment of the induced effect of selected iron hydroxysulfates biosynthesized using *Acidithiobacillus ferrooxidans* for biomineralization of acid mine drainage. *Water Sci. Technol.* **2023**, *87*, 1879–1892. [CrossRef] [PubMed]
46. Chen, Y.; Huang, F.; Xie, X.Y. Effect of simulated inorganic anion leaching solution of electroplating sludge on the bioactivity of *Acidithiobacillus ferrooxidans*. *J. Environ. Sci.* **2014**, *35*, 1377–1383.
47. Liu, F.W.; Qiao, X.X.; Xing, K.; Shi, J.; Zhou, L.X.; Dong, Y.; Bi, W.L.; Zhang, J. Effect of Nitrate Ions on *Acidithiobacillus ferrooxidans*-Mediated Bio-oxidation of Ferrous Ions and Pyrite. *Curr. Microbiol.* **2020**, *77*, 1070–1080. [CrossRef]
48. Fryi, V.; Lazarof, F.N.; Packer, L. Sulfate-dependent iron oxidation by *Thiobacillus ferrooxidans*: Characterization of a new EPR detectable electron transport component on the reducing side of rusticyanin. *Arch. Biochem. Bio* **1986**, *246*, 650–654. [CrossRef]
49. Gramp, J.P.; Jones, F.S.; Bigham, J.M.; Tuovinen, O.H. Monovalent cation concentrations determine the types of Fe(III) hydroxysulfate precipitates formed in bioleach solutions. *Hydrometallurgy* **2008**, *94*, 29–33. [CrossRef]
50. Huang, H.; Geng, K.; Wang, C.; Wu, X.; Wei, C. Impact of Fulvic Acid and *Acidithiobacillus ferrooxidan* Inoculum Amount on the Formation of Secondary Iron Minerals. *Int. J. Environ. Res. Public Health* **2023**, *20*, 4736. [CrossRef]
51. Karamanov, A.; Pelino, M. Evaluation of the degree of crystallisation in glass-ceramics by density measurements. *J. Eur. Ceram. Soc.* **1999**, *19*, 649–654. [CrossRef]
52. Sun, Z.P.; Ni, Y.; Yue, W.Q.; Yan, F.; Liu, F.W.; Li, X.W. Preparation of silver nanoparticles loaded Schwertmannite and catalytic degradation performance on methyl orange. *Acta Sci. Circumstantiae* **2022**, *42*, 61–70.
53. Zhang, Z.; Wang, L.; Zhou, B.; Wang, S.; Fan, L.; Hu, S.; Wu, Y. Adsorption Performance and Mechanism of Synthetic Schwertmannite to Remove Low-Concentration Fluorine in Water. *Bull. Environ. Contam. Toxicol.* **2021**, *107*, 1191–1201. [CrossRef] [PubMed]
54. Dutrizac, J.E. Factors affecting alkali jarosite precipitation. *Metall. Trans. B* **1983**, *14*, 531–539. [CrossRef]
55. Regenspurg, S.; Brand, A.; Peiffer, S. Formation and stability of schwertmannite in acid mining lakes. *Geochim. Cosmochim Acta* **2004**, *68*, 1185–1197. [CrossRef]
56. Gaowa, N.; Hironori, O.; Shuqin, B.; Kotaro, Y.; Takushi, Y. Uptake mechanism of silicic acid by schwertmannite and its stabilization. *J. Environ. Chem. Eng.* **2023**, *11*, 111136.
57. Bigham, J.; Schwertmann, U.; Traina, S.; Winland, R.; Wolf, M. Schwertmannite and the chemical modeling of iron in acid sulfate waters. *Geochim. Cosmochim Acta* **1996**, *60*, 2111–2121. [CrossRef]